Appl. Phys. B 83, 579–585 (2006)
DOI: 10.1007/s00340-006-2209-y

Applied Physics B
Lasers and Optics

H. WANG[1,2]
G. JIA[1,2]
F. YANG[1]
Y. WEI[1]
Z. YOU[1]
Y. WANG[1]
J. LI[1,2]
Z. ZHU[1,2]
X. LU[1,2]
C. TU[1,✉]

Growth and spectral properties of Tm^{3+}-doped $NaGd(WO_4)_2$ crystal

[1] Fujian Institute of Research on the Structure of Matter, Chinese Academy of Sciences, Fuzhou, Fujian 350002, P.R. China
[2] Graduated School of Chinese Academy of Sciences, Beijing 100039, P.R. China

Received: 17 January 2006/Revised version: 2 March 2006
Published online: 14 April 2006 •

ABSTRACT Thulium doped sodium gadolinium tungstate crystals with sizes of about 20 mm × 45 mm were grown successfully by the Czochralski technique along the (001) orientation. X-ray powder diffraction (XRD) of sodium gadolinium tungstate was described and the linear thermal expansion coefficients for the *c*- and *a*-axes were measured as 1.60×10^{-5} and 7.89×10^{-6} °C^{-1}. Polarized absorption spectra, and fluorescence spectra, as well as fluorescence decay curves of Tm^{3+}-doped $NaGd(WO_4)_2$, have been recorded at room temperature and used to calculate the absorption and stimulated emission cross-sections. Based on the Judd–Ofelt theory, three intensity parameters were obtained. The luminescent quantum efficiency of the $^3H_4$ level was determined to be approximately 65% for this material. The emission cross-section of the $^3F_4 \rightarrow {}^3H_6$ IR transition at about 1.8 μm was estimated by the reciprocity method.

PACS 78.55.Hx; 65.40.De; 78.20.-e

1 Introduction

Na-based double tungstates have less destructive phase transitions than those observed in K-based double tungstates. Due to this reason the crystal growth of $NaRE(WO_4)_2$ (where RE stands for rare earth) compounds by the Czochralski (CZ) method, which allows obtaining of crystals of large sizes at high growth-rates, has attracted attention in the last few years for use in RE-doped systems [1–5]. There is a technological interest in Tm^{3+} doped crystals and glasses because of their potential applications as a laser active media with emissions in the visible and mid-infrared spectral regions. The absorption peak at about 800 nm corresponding to the $^3H_6 \rightarrow {}^3H_4$ transition suggests that Tm^{3+}-doped sodium gadolinium tungstates are promising candidates for GaAlAs laser diode (LD) pumping [6]. The higher efficient emissions at near infrared are also very interesting due to cross-relaxation processes between Tm^{3+} ions [7]. In particular, the 1.8 μm laser emission meets a great interest in many fields and applications like optical communications, coherent laser radar and medical equipment [8–13].

The $NaGd(WO_4)_2$ (NGW) single crystal, one of the excellent laser host materials, belongs to the tetragonal system with the space group of $I4_1/a$. It has the scheelite ($CaWO_4$) structure. The cell parameters are as follows: $a = b = 5.243$ Å, $c = 11.384$ Å [14], $\alpha = \beta = \gamma = 90°$, $V = 312.28$ Å^3, $Z = 4$, $d = 7.2$ g/cm^3 [15]. The melting point is 1253 °C [16]. The crystal structure of NGW is shown in Fig. 1 [17].

In this paper, crystal growth, X-ray powder diffraction (XRD) analysis and linear thermal expansion coefficients are described. The present paper is also devoted to investigating the spectroscopic properties of Tm^{3+}-doped NGW crystal.

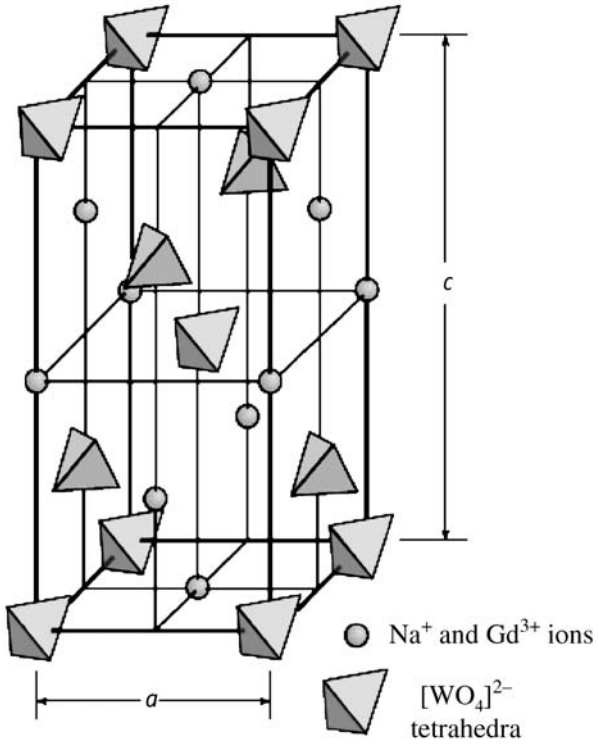

FIGURE 1 Crystal structure of $NaGd(WO_4)_2$

✉ Fax: +86-591-8371-4946, E-mail: tcy@fjirsm.ac.cn

2 Experimental

Tm^{3+}-doped NGW crystal was grown by the Czochralski technique (shown in Fig. 2). The concentration of thulium ions in the crystal was measured to be 0.628 wt. % by the inductively coupled plasma-atomic emission spectrometry (ICP–AES) method.

XRD investigations were carried out with a CAD4 diffractometer equipped with Cu K_α radiation ($\lambda = 1.054056$ Å). The data was collected using a Ni-filtered Cu-target tube at room temperature in the 2θ range of 5–85°. The X-ray powder diffraction pattern is shown in Fig. 3. The XRD pattern was in good accordance with the standard JCPDS card of $NaGd(WO_4)_2$ (No.25-0829).

The crystal was oriented by a YX-2 X-ray crystal orientation unit (Dandong) and the exact orientation of the grown crystal was determined by X-ray Laue back-reflection technique. Thermal expansion coefficients of Tm^{3+}: NGW along the crystallographic axes were measured by a Diatometer 402 PC in the temperature range of 400–1000 °C. The oriented sample lengths of the two crystallographic a- and c-axes were 3.00 and 9.60 mm, respectively. The sample was kept in a fused silica sample holder and heated at a rate of 10 °C/min in the standard air atmosphere.

Room temperature absorption spectra of these crystals were recorded by a Perkin-Elmer UV-VIS-NIR Spectrometer (Lambda-900). The emission spectrum of the crystal was recorded at room temperature by an Edinburgh Instruments FLS920 spectrophotometer.

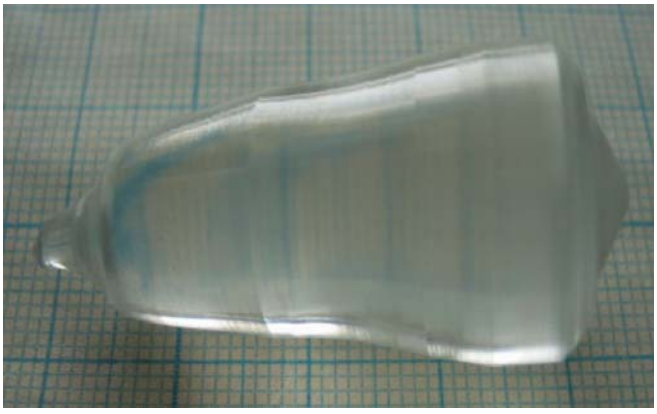

FIGURE 2 Picture of Tm^{3+}:$NaGd(WO_4)_2$ crystal

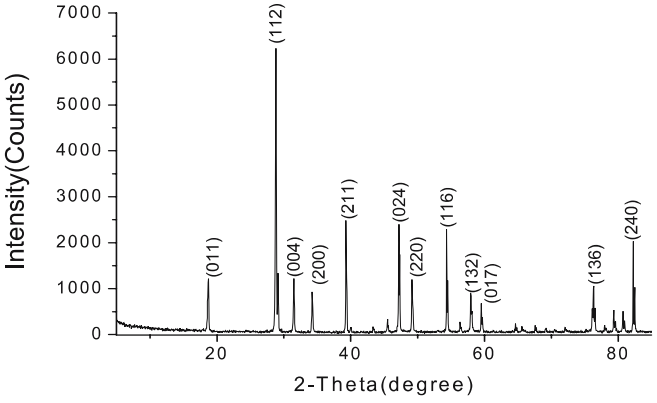

FIGURE 3 X-ray powder diffraction pattern of $NaGd(WO_4)_2$ crystal

3 Results and discussion

3.1 *Crystal growth*

Tm^{3+}-doped NGW crystal was grown by the Czochralski technique. The NGW compound was prepared by classical solid-state reaction. The starting materials were prepared by mixing analytical grade Na_2CO_3, WO_3, spectral grade Gd_2O_3, and 4N purity Tm_2O_3 powders according to the formula of $NaGd_{0.96}Tm_{0.04}(WO_4)_2$. The $NaGd_{0.96}Tm_{0.04}(WO_4)_2$ were synthesized according to the following reactions:

$$0.5Na_2CO_3 + 0.48Gd_2O_3 + 2WO_3 + 0.02Tm_2O_3 = NaGd_{0.96}Tm_{0.04}(WO_4)_2 + 0.5CO_2\uparrow .$$

These compounds were ground, mixed separately in the molar ratio in an agate mortar and pressed into pieces. Then they were put into a platinum crucible of diameter 80 mm and a height of 80 mm. They were slowly heated to 1080 °C and maintained at this temperature for three days. They were then ground, mixed and heated again. The above process was repeated to make sure that the chemicals reacted thoroughly. It was then placed in an Iridium (Ir)-crucible and heated in a DJL-400 furnace. It was heated up to a temperature 50 °C higher than the crystallization temperature for about 2 h so as to ensure it melted completely and homogeneously. During crystal growth, the Ir rod rotated at a rate of 11 rpm and the pulling rate was 0.4–1.2 mm/h. When these procedures were over, the crystals were drawn out of the melt and cooled down to room temperature at a rate of 12–30 °C/h. The growth parameters are displayed in Table 1.

3.2 *Segregation coefficients*

The calculation of segregation coefficients of the dopant in crystals, K, was performed by the following formula:

$$K = \frac{(\text{molesTm}/(\text{molesTm} + \text{molesGd}))\text{crystal}}{(\text{molesTm}/(\text{molesTm} + \text{molesGd}))\text{melt}} . \quad (1)$$

Here molesTm and molesGd are the mole fraction of dopant and trivalent host ion, respectively, in the crystal (numerator) and in the melt (denominator). The segregation coefficient of Tm in NGW appeared to be 0.63. It is not equal to unity due to the different radii between thulium ions and host component gadolinium ions ($r_{Tm^{3+}} = 1.04$ Å, $r_{Gd^{3+}} = 1.11$ Å).

Parameters	Property	Parameters	Property
Seeding temp. (°C)	1267	Atmosphere	N_2
Soaping temp. (°C)	1317	Growth rate (mm/h)	1–1.2
Soaping time (h)	2	Rotation rate (rpm)	11
Crucible size (mm)	$\varnothing = 55 \times 30$	Crucible materials	Iridium

TABLE 1 Growth conditions of Tm^{3+}-doped NGW

3.3 *Thermal expansion*

As a significant part of the pump power is converted into heat inside the material during laser operation, it is important to know its linear thermal expansion coefficients to predict how the material behaves when the temperature increases [18]. The thermal expansion coefficients of the crystal are important factors for crystal growth too. NGW belongs to the tetragonal crystal system with two independent principal thermal expansion components whose matrix for the thermal expansion tensor is

$$\alpha_{ij} = \begin{pmatrix} a_1 & 0 & 0 \\ 0 & a_2 & 0 \\ 0 & 0 & a_3 \end{pmatrix} .$$

The thermal components α_1 ($\alpha_1 = \alpha_2$) and α_3 can be determined by measuring the thermal expansion along the a- and c-oriented samples. From the experimental results, we got

$$\alpha_{ij(\mathrm{NGW})} = \begin{pmatrix} 7.89 & 0 & 0 \\ 0 & 7.89 & 0 \\ 0 & 0 & 16.0 \end{pmatrix} \times 10^{-6}\,^{\circ}\mathrm{C}^{-1} .$$

The figure of linear expansions versus temperature is shown in Fig. 4 from which we can see that the thermal expansion coefficients along the a- and c-axes are positive in the measuring temperature range of 400–1000 K. The linear thermal expansion coefficient is defined as:

$$\alpha = \frac{1}{L_0}\frac{\mathrm{d}L}{\mathrm{d}T} . \qquad (2)$$

Here L_0 is the initial length of the sample at room temperature and ΔL is the change in length when the temperature changes ΔT. We can calculate the thermal expansion coefficient from the slope of the linear fitting of the linear relationship between $\mathrm{d}L/L_0$ and the temperature. So the linear thermal expansion coefficients for c- and a-axes are 1.60×10^{-5} and $7.89 \times 10^{-6}\,^{\circ}\mathrm{C}^{-1}$, respectively.

From Fig. 1 we can see that one unit cell of four layers of ions lies along the c-axis direction while only two layers lie along the a-axis direction. Thus, ions are more compressible in the a-axis direction than those in the c-axis direction. As a result, when the NGW crystal is heated, a relatively larger thermal expansion occurs in the c-axis direction due to the increase of thermal vibration of ions inside. Therefore, we should grow the crystal along the c-axis to avoid the cracking.

3.4 *Spectrum characteristics*

The oriented crystal was cut into several samples and optically polished to flat and parallel faces. The thickness of the samples was 1.20 mm. The polarized absorption spectrum of $NaGd(WO_4)_2$:Tm^{3+} crystal is shown in Fig. 5. The most interesting aspect of the absorption spectra was the intensive absorption bands at about 795 nm, which were suitable for pumping of commercial GaAlAs laser diode. The absorption cross section σ_a can be determined by the following equation:

$$\sigma_a = \alpha / N_c . \qquad (3)$$

Here α is the absorption coefficient, $\alpha = A/L \times \log \mathrm{e}$, A is the absorbance, L is the thickness of the polished crystal, and N_c

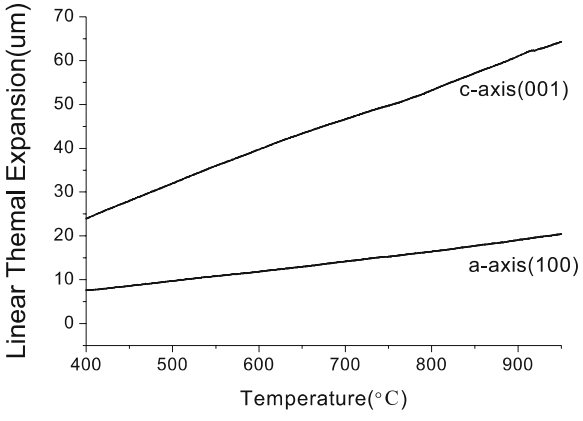

FIGURE 4 Linear thermal expansions as a function of temperature along the c- and a-axes

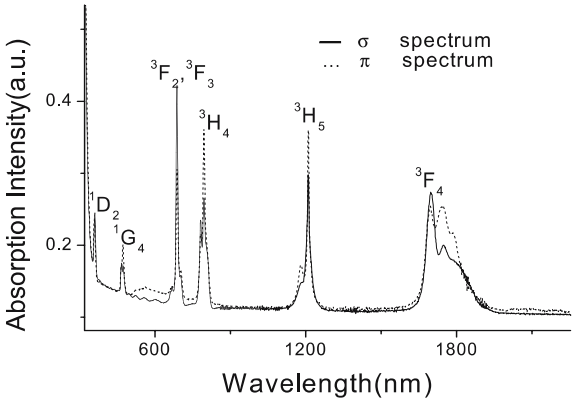

FIGURE 5 Polarized absorption spectrum of Tm^{3+}-doped NGW crystal

Crystal	Polarization Spectrum	Wavelength (nm)	FWHM (nm)	Cross-section (10^{-20} cm^2)	Ref.
5 at. % Tm:YVO_4	π	797.5	5	2.5	[19]
0.5 at. % Tm: $LiTaO_3$	σ	795	9.5	6	[20]
0.7 at. % Tm:$KYb(WO_4)_2$	π	793.6	3.5	8.8	[21]
	σ	801.8	1.4	4.8	
3 at. % Tm:$KGd(WO_4)_2$	π	795	–	8.5	[22]
	σ	795	–	3.0	
0.628 wt. % Tm:NGW	π	795	5	3.16	This work
	σ	795	9	4.30	

TABLE 2 Comparison between the FWHM and absorption cross-section in Tm^{3+}-doped crystal

is the rare-earth ions concentration in atoms. For the π polarization spectrum, the most intense absorption centered at 795 nm has an absorption coefficient of 5.09 cm^{-1} and a 5 nm full width at half maximum (FWHM), while for the σ polarization spectrum, the most intense absorption is situated at 795 nm too, which has an absorption coefficient of 6.92 cm^{-1} and a 9 nm FWHM. The thulium ions concentration in the crystal is 0.628 wt. %, so $N_c = 1.61 \times 10^{20}\,cm^{-3}$. Thereby, the absorption cross-section value is $3.16 \times 10^{-20}\,cm^2$ for the π polarization spectrum, while it is $4.30 \times 10^{-20}\,cm^2$ for the σ polarization spectrum. Table 2 gives the parameters of the FWHM and cross-section σ_a of some other Tm^{3+}-doped crystals for comparison. We can see that Tm^{3+}:NGW has a moderate absorption cross section and FWHM which suggests that it is preferable to pump Tm^{3+}:NGW crystals by a GaAlAs laser diode.

The experimental data obtained from the polarized absorption spectra were used to calculate the oscillator strengths. The measured absorption line strengths $S_{JJ'}$ for transitions from the ground state $^3H_6$ manifold ($J = 6$ in Tm^{3+}) to the excited J'-manifold can be obtained from the absorption spectra using the following expression reported in [23]:

$$S_{\text{meas}}(J \to J') = \frac{3ch(2J+1)\Gamma_\pi + 2\Gamma_\sigma}{8\pi^3 N_0 \lambda\, e^2 \chi_\pi + 2\chi_\sigma}. \quad (4)$$

Here N_0 is the Tm^{3+} concentration in the crystal, λ is the mean wavelength of the absorption band, c is the vacuum speed of light, J is the total angular momentum of the ground state ($J = 6$ in Tm^{3+}), $\chi_{\sigma,\pi} = (n^2_{\sigma,\pi} + 2)^2/9n\sigma\pi$ is the Lorentz local field correction for the refractivity of the medium (here the mean refractive index of NGW is 1.945 [24]) and Γ is the integrated absorbance for each absorption band, which can be determined by

$$\Gamma = \frac{\int D(\lambda)\,d\lambda}{L \log e} = \frac{2.303 \int D(\lambda)\,d\lambda}{L}. \quad (5)$$

Here L is the crystal thickness and $D(\lambda)\,d\lambda$ is the measured optical density as a function of wavelength. Table 3 presents the integrated absorbance, electrical dipole line strengths and oscillator strengths of the Tm^{3+}:NGW crystal.

Based on the Judd–Ofelt theory, the measured line strengths were then used to obtain the J–O intensity parameters Ω_2, Ω_4 and Ω_6 by fitting the set of equations from the corresponding transitions between J and J' manifolds in the following equation:

$$S_{\text{calc}}(J \to J') = \sum_{t=2,4,6} \Omega_t \left|\left\langle (S, L) J \left\| U^{(t)} \right\| (S', L') J' \right\rangle\right|^2. \quad (6)$$

Here $U^{(t)}(t = 2, 4, 6)$ are the matrix elements of the unit tensor calculated by Carnall et al. [25]. The root mean square (rms) deviation between experimental and calculated strengths was determined by

$$\text{rms}\,\Delta S = \sqrt{\sum_{i=1}^{N} \left(S_{\text{meas}} - S_{\text{calc}}\right)^2/(N-3)}. \quad (7)$$

Where

$$\text{rms} S = \sqrt{\sum_{i=1}^{N} S^2_{\text{meas}}/N}. \quad (8)$$

So the rms error is $0.496 \times 10^{-20}\,cm^2$.

After a least-square fitting of S_{meas} to S_{calc}, the three J–O intensity parameters were obtained: $\Omega_2 = 5.0 \times 10^{-20}$, $\Omega_4 = 1.3 \times 10^{-20}$, $\Omega_6 = 4.6 \times 10^{-20}\,cm^2$. The three J–O intensity parameters of other Tm^{3+}-doped crystals are given in Table 4 and we can see that Tm^{3+}: $NaGd(WO_4)_2$ crystal has higher values of Judd–Ofelt parameters.

The experimental oscillator strength f_{exp} can be calculated by using the following formula:

$$f_{\text{exp}} = \frac{mc^2}{\pi e^2 N_0 L \lambda^2}\Gamma. \quad (9)$$

From the $4f$–$4f$ intensity model [31], the calculated oscillator strength of a transition between two multiplets is given

Excited states	λ (nm)	Γ(nm/cm)			Line strength ($10^{-20}\,cm^2$)		Oscillator strength (10^{-6})	
		σ	π	Average	S_{exp}	S_{calc}	f_{exp}	f_{cal}
$^3F_4$	1744	184.87	164.96	178.23	4.479	3.779	4.112	3.469
$^3H_5$	1210	129.7	127.07	128.82	4.666	4.757	6.174	6.295
$^3H_4$	795	73.46	66.58	71.17	3.924	4.067	7.902	8.189
$^3F_3 + {}^3F_2$	688	56.80	68.40	60.67	3.865	4.286	8.994	9.974
$^1G_4$	473	6.84	4.48	6.05	0.561	0.399	1.898	1.352
$^1D_2$	360	7.42	9.24	8.03	0.978	0.848	4.348	3.77

TABLE 3 Integrated absorbance, electrical dipole line strengths and oscillator strengths of Tm^{3+}:NGW crystal

Crystal	Ω_2 ($10^{-20}\,cm^2$)	Ω_4 ($10^{-20}\,cm^2$)	Ω_6 ($10^{-20}\,cm^2$)	Ref.
$Tm:Y_2O_3$	4.07	1.46	0.61	[26]
$Tm:YVO_4$	1.94	0.158	0.396	[27]
$Tm:SrGdGa_3O_7$	1.29	1.08	0.47	[28]
$Tm:CaYAlO_4$	1.55	3.45	1.18	[29]
$Tm:KGd(WO_4)_2$	2.64	5.84	14	[30]
Tm:NGW	5.012	1.355	4.594	This work

TABLE 4 The J–O intensity parameters of Tm^{3+}-doped crystals

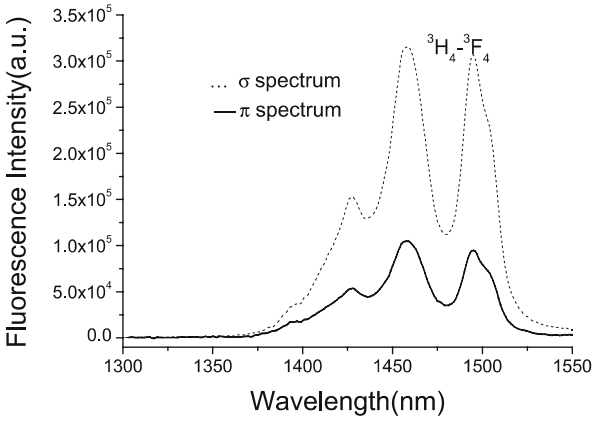

FIGURE 6 Polarized room temperature fluorescence spectrum of Tm^{3+}: NGW crystal excited by 795 nm light

by:

$$f_{\text{calc}} = \frac{8\pi^2 mc}{3h\lambda(2J+1)}\frac{(n^2+2)^2}{9n} \times \sum_{t=2,4,6} \Omega_t \left\langle 4f^N(\alpha' S' L')J' \left\| U^{(t)} \right\| 4f^N(\alpha SL)J \right\rangle^2 . \quad (10)$$

The experimental oscillator strength f_{exp} can be obtained through the absorption spectrum and (9). The results are also listed in Table 3.

The emission spectrum of the crystal recorded at room temperature is shown in Fig. 6. As can be seen from this figure, the intense emission peaks are centered at 1457 nm, corresponding to the transition $^3H_4 \rightarrow {}^3F_4$ of Tm^{3+} ions.

Using the obtained emission line strengths, the radiative decay rates $A(J \rightarrow J')$ can be determined by the following expressions [32]:

$$A(J \rightarrow J') = \frac{64\pi^4 e^2}{3h(2J+1)\overline{\lambda^3}}\frac{n(n^2+2)^2}{9} \times \sum_{t=2,4,6} \Omega_t \left| \left\langle (S,L)J \left\| U^{(t)} \right\| (S',L')J' \right\rangle \right|^2 \quad (11)$$

$$A_T(J) = \sum_{J'} A(J \rightarrow J'). \quad (12)$$

Then the radiative lifetimes $\tau_R = 1/A_T(J)$, so the mathematical formula for the fluorescent branching ratio is given by [32]:

$$\beta(J') = \frac{A(J \rightarrow J')}{A_T(J)}. \quad (13)$$

The calculated radiative transition rate, the branching ratios and the radiative lifetime for different transition levels are presented in Table 5. The stimulated emission cross-section σ_P related to the radiative transition probability can be defined by

$$\sigma_P = \frac{A(J \rightarrow J')\lambda_P^2}{4\pi^2 n^2 c\Delta\nu}. \quad (14)$$

Here $\Delta\nu$ is the full frequency width at half maximum, λ_P is the vacuum wavelength of the emission peak. Therefore, the emission cross-section σ_P of π and σ emission spectra

Start levels	Terminal levels	Wavelength (nm)	A (s^{-1})	β	τ (μs)
$^1D_2$	$^3H_6$	360	19.020	0.299	16
	$^3F_4$	454	35.210	0.554	
	$^3H_5$	512	610	0.010	
	$^3H_4$	658	6.125	0.096	
	$^3F_3 + {}^3F_2$	755	2.246	0.035	
	$^1G_4$	1506	368	0.006	
$^1G_4$	$^3H_6$	473	2.079	0.281	135
	$^3F_4$	649	731	0.099	
	$^3H_5$	777	3.423	0.463	
	$^3H_4$	1168	915	0.124	
	$^3F_3 + {}^3F_2$	1514	250	0.034	
$^3H_4$	$^3H_6$	795	4.514	0.923	204
	$^3F_4$	1461	343	0.07	
	$^3H_5$	2318	36	0.007	
$^3F_4$	$^3H_6$	1744	551	1	18 160

TABLE 5 Calculated radiative transition rate, branching ratios and radiative lifetime for different transition levels of Tm^{3+}:NGW crystal

centered at 1457 nm were measured to be 5.59×10^{-21} and 5.41×10^{-21} cm^2, respectively.

Figure 7 presents the luminescence decay curves excited by 795 nm at room temperature in correspondence with the emission line $^3H_4 \rightarrow {}^3F_4$ at 1457 nm. The fluorescence lifetime τ_f is measured to be 133 μs. The value can be compared with those of YVO_4: 130 μs and 100 μs respectively for 0.5% and 1% Tm and of Y_2O_3: 270 μs and 190 μs respectively for 0.5% and 1% Tm [26]. The radiative lifetime τ_r of the $^3H_4$ level of Tm^{3+}:NGW crystal is calculated to be 204 μs. The linear relationship in the figure appears as a single exponential behavior, and the fluorescence life time could be obtained from the slope of the fitting line. So the luminescent quantum efficiency of the $^3H_4$ level is $\eta = \tau_f/\tau_r = 133/204 = 65\%$. We can see that Tm^{3+}:NGW crystal has a large luminescent quantum efficiency.

The electronic configuration of Tm^{3+} is $4f^{12}$ and the lower and upper electronic states identified as $^3F_4 \rightarrow {}^3H_6$ (1.8 μm) has been of great interest for many years. The most important parameter influencing the potential laser performance of a material is the emission cross section, which can be determined from the spectroscopic data by the reciprocity method (RM) [33, 34].

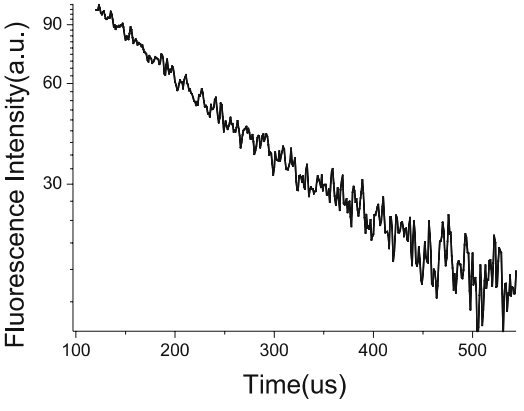

FIGURE 7 Room temperature luminescence decay curves excited by 795 nm light

The reciprocity method is based on deriving the emission cross section from the absorption spectra, the impurity concentration, and a detailed knowledge of the energy levels of the system. The emission cross-section (σ_{em}) is calculated from the absorption cross-section (σ_{abs}), and the splitting of the energy levels using the following equation:

$$\sigma_{em}(\lambda) = \sigma_{abs}(\lambda)\frac{Z_l}{Z_u}\exp[(E_{ZL} - hc/\lambda)/k_B T]\,. \quad (15)$$

Here $\sigma_{abs} = \alpha/N_0$ is the absorption cross section, N_0 is the dopant concentration, Z_l and Z_u are the partition functions of the lower and upper levels, and E_{ZL} is the zero-line or energy separation between the lowest energy sublevels of the ground state (lower) and the first excited state (upper), respectively.

In order to calculate the partition functions, energies of all the crystal-field components of the $^3H_6$ and $^3F_4$ states are required. The missing components are accounted for by scaling the calculated function Z_{calc} according to the following equation [35]:

$$Z(\text{scaled}) = Z(\text{calc}) \times \frac{n_{exp}}{n_{obs}}\,. \quad (16)$$

Here n_{exp} and n_{obs} are the number of levels expected and the number of levels observed, respectively. However, due to a lack of low temperature emission spectra, the precise energy scheme of Tm^{3+}:$NaGd(WO_4)_2$ can not be obtained at present. In our case, we estimated that $\frac{Z_l}{Z_u} = 1.21$ and E_{ZL} was $5605\,cm^{-1}$ respectively, which is of the order of those of Tm^{3+}:LaF_3, Tm^{3+}:$Y_3Al_5O_{12}$, Tm^{3+}:$YAlO_3$, Tm^{3+}:$KCaF_3$ [35], Tm^{3+}: $KGd(WO_4)_2$ [36], and Tm^{3+}: $KYb(WO_4)_2$ [37] crystals.

The polarized absorption and emission cross-sections calculated by the RM method are shown in Fig. 8a and b. The emission cross-section at 1.745 μm was $\sigma_{em} = 3 \times 10^{-20}\,cm^2$ for the σ polarization spectrum, while $\sigma_{em} = 4.6 \times 10^{-20}\,cm^2$ for the π polarization spectrum. These values are higher than that of Tm^{3+}:$KGd(WO_4)_2$ [$3 \times 10^{-20}\,cm^2$ at 1.838 μm and $1.9 \times 10^{-20}\,cm^2$ at 1.756 um] [36]. The emission cross-section was magnified at longer wavelengths due to the shortcoming of the reciprocity method. In the long-wavelength wing of an absorption spectrum the absorption intensity is low and influenced by a noise, which is substantially magnified by the exponential factor of (15) [38].

The transition of $^3F_4 \rightarrow {}^3H_6$ corresponds to a quasi-three level laser scheme in which the lower level is thermally populated at room temperature. The reabsorption and the increasing of the threshold may come forth during the laser operation. Reducing the reabsorption and maintaining the efficient absorption of the pump light is important in the design of the thulium doped laser systems on the $^3F_4 \rightarrow {}^3H_6$ transition [36].

If P is the population inversion rate, the gain cross section can be calculated using the following formula [33, 39]:

$$\sigma_{gain} = P\sigma_{em}(\lambda) - (1 - P)\sigma_{abs}(\lambda)\,. \quad (17)$$

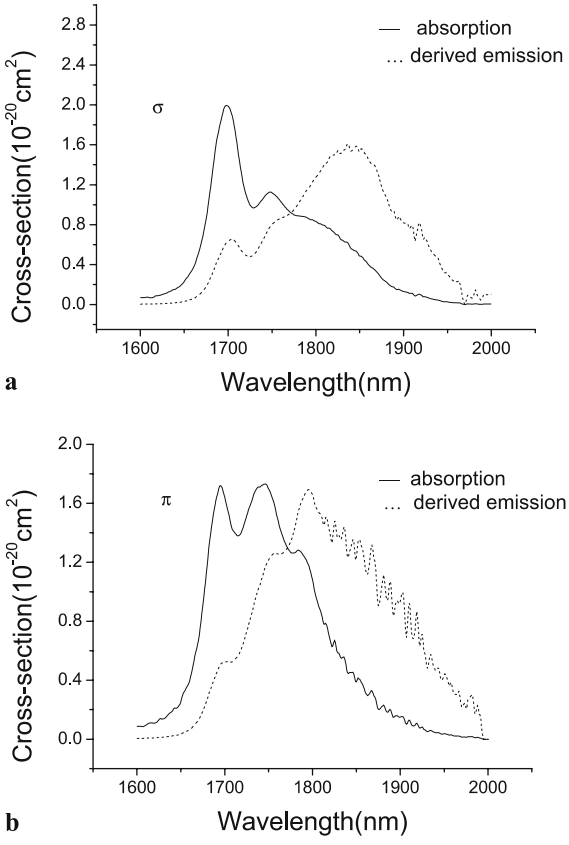

FIGURE 8 Polarized absorption and emission cross-sections corresponding to the $^3H_6 \rightarrow {}^3F_4$ transition for (**a**) σ polarization; (**b**) π polarization

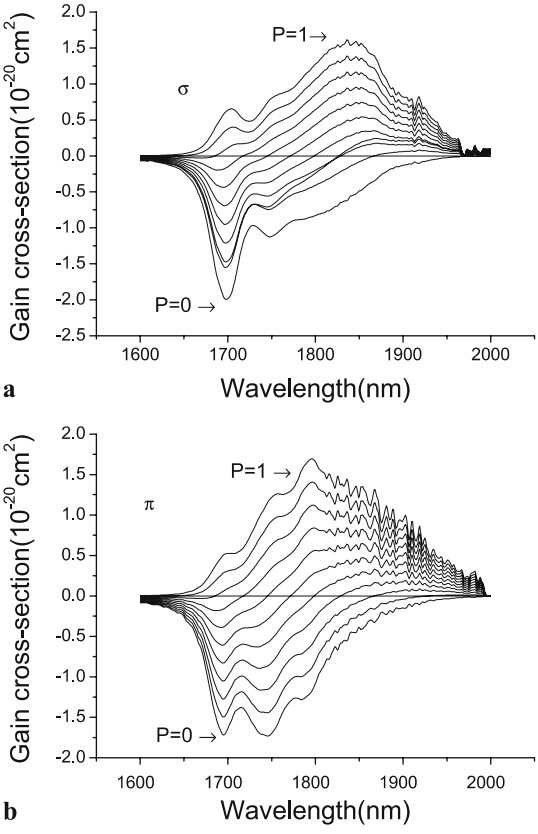

FIGURE 9 Gain cross-section calculated for different values of P for the $^3F_4 \rightarrow {}^3H_6$ transition for (**a**) σ polarization; (**b**) π polarization

Here σ_{em} and σ_{abs} are the emission and absorption cross sections derived from the RM method, respectively. The wavelength dependencies of the gain cross section were calculated in the terms of population inversion P ($P = 0$, 0.1, 0.2, ..., 1) and are shown in Fig. 9a and b. The population inversion rate needed to achieve amplification is expected to be higher than 0.2. For a population inversion level of 0.3, the gain is produced in the 1.79–2.0 μm spectral regions. The higher energy limit of this interval increased when the population inversion level was increased, reaching up to 1.75 μm for a population inversion level of 0.5. For this level the maximum gain cross-section value is 0.5×10^{-20} cm^2 at 1.867 μm for σ polarization and 0.4×10^{-20} cm^2 at 1.826 μm for π polarization. Laser experiments for this emission are expected to find light amplification in future at this point.

4 Conclusion

A new laser crystal, Tm^{3+}:$NaGd(WO_4)_2$ crystal with dimensions of 20 mm × 45 mm was grown successfully by the Czochralski technique. Polarized absorption and emission spectra of Tm^{3+}-doped $NaGd(WO_4)_2$ were presented. We measured the FWHM and calculated the absorption cross-section centered at about 795 nm of Tm^{3+}:$NaGd(WO_4)_2$ crystals. Favorable values of FWHM and absorption cross-section suggest that Tm^{3+}:$NaGd(WO_4)_2$ crystals are promising candidates for LD pumping.

We applied J–O theory to calculated J–O intensity parameters, radiative probabilities, radiative branching ratios as well as radiative time. Tm^{3+}:$NaGd(WO_4)_2$ crystal has large J–O intensity parameters and luminescent quantum efficiency. The fluorescence lifetime corresponding to the emission line $^3H_4 \rightarrow {}^3F_4$ at 1457 nm is 133 μs. Tm^{3+}:$NaGd(WO_4)_2$ crystal may be a potential candidate for 1.5 μm lasers.

The emission cross-section at 1.8 μm was estimated using the reciprocity method from the room temperature polarized absorption spectra. The emission cross-section of the $^3F_4 \rightarrow {}^3H_6$ IR transition is high which implies possible laser oscillation at about 1.8 μm. The optical gain for several population inversion rates was estimated to determine the spectral region in which light amplification is possible for future laser experiments. From the gain versus wavelength, we found a tuning range of 1.79–2.0 μm for the $^3F_4 \rightarrow {}^3H_6$ transition.

ACKNOWLEDGEMENTS This work was supported by the Innovative Project of the Chinese Academy of Sciences (KJCX2-SW-h05), the Nature Science Foundation of Fujian Province of China (E0410028), and the Frontier & Interdisciplinary project of the Fujian Institute of Research on the Structure of Matter, CAS.

REFERENCES

1 M.D. Serrano, F. Esteban-Betegón, C. Zaldo, J. Cryst. Growth **275**, 819 (2005)
2 Z. Cheng, Q. Lu, S. Zhang, J. Liu, X. Yi, F. Song, Y. Kong, J. Han, H. Chen, J. Cryst. Growth **222**, 797 (2001)
3 J. Hanuza, L. Macalik, M. Mczka, E.T.G. Lutz, J.H. van der Maas, J. Mol. Struct. **511–512**, 85 (1999)
4 V. Volkov, C. Zaldo, J. Cryst. Growth **206**, 60 (1999)
5 P.V. Klevtsov, R.F. Klevtsova, J. Solid State Chem. **2**, 278 (1970)
6 C. Tu, Chin. J. Synth. Cryst. **302**, 135 (2001)
7 K. Ohta, H. Saito, M. Obara, J. Appl. Phys. **73**, 3149 (1993)
8 S.W. Henderson, C.P. Hale, J.R. Magee, M.J. Kavaja, A.V. Huffeker, Opt. Lett. **16**, 773 (1991)
9 S.W. Henderson, K. Ota, Rev. Laser Eng. **25**, 19 (1997)
10 H.P. Weber, M. Frenz, H. Pratisto, M. Ith, R. Hausler, P. Schar, Laser Phys. **8**, 785 (1998)
11 T. Schweizer, B.N. Samson, J.R. Hector, W.S. Brocklesby, D.W. Hewak, D.N. Payne, Infrared Phys. Technol. **40**, 329 (1999)
12 R. Kaufman, A. Hartmann, R. Hibst, J. Dermatol. Surg. Oncol. **20**, 112 (1994)
13 K. Miazato, D.F. de Sousa, A. Delben, J.R. Delben, S.L. de Oliveira, L.A.O. Nunes, J. Non-Cryst. Solids **273**, 246 (2000)
14 M.V. Mokhosoev, V.I. Krivobok, S.M. Aleikina, Neorg. Mater **3**, 1657 (1967)
15 N. Faure, C. Borel, M. Couchaud, Appl. Phys. B **63**, 593 (1996)
16 E.Y. Rode, V.N. Karpov, M.M. Ivanova, Zh. Neorg. Khim. **16**, 1713 (1971)
17 Y.K. Voron'ko, E.V. Zharikov, D.A. Lis, Inorg. Mater. **39**, 1308 (2003)
18 J.J. Carvajal, R. Sole, J. Gavalsa, J. Massons, F. Diaz, M. Aguilo, Chem. Mater. **15**, 2730 (2003)
19 K. Ohta, H. Saito, M. Obara, J. Appl. Phys. **73**, 3149 (1993)
20 I. Sokolska, W. Ryba-Romanowski, S. Golab, M. Baba, M. Swirkowicz, T. Lukasiewicz, J. Phys. Chem. Solids **61**, 1573 (2000)
21 M.C. Pujol, F. Güell, X. Mateos, J. Gavaldà, R. Solé, J. Massons, M. Aguiló, F. Díaz, Phys. Rev. B **66**, 144 304 (2002)
22 F. Güell, X. Mateos, J. Gavaldà, R. Solé, M. Aguiló, F. Díaz, M. Galan, J. Massons, Opt. Mater. **25**, 71 (2004)
23 D. Jaque, O. Enguita, U. Caldino, M.O. Ramirez, J. Garcia Sole, J. Appl. Phys. **90**, 561 (2001)
24 M. Rico, J. Liu, U. Griebner, V. Petrov, Opt. Express **12**, 5362 (2004)
25 W.T. Carnall, P.R. Fields, K. Rajnak, J. Chem. Phys. **49**, 4424 (1968)
26 F.S. Ermeneux, C. Goutaudier, R. Moncorgé, Opt. Mater. **8**, 83 (1997)
27 F. Song, H. Guo, W. Zhang, Spectrosc. Spectral Anal. **221**, 1 (2001)
28 B. Chen, Acta Photon. Sin. **287**, 667 (1999)
29 R. Moncorgé, N. Garnier, P. Kerbrat, Opt. Commun. **141**, 29 (1997)
30 C. Tu, J. Li, Z. Zhu, Opt. Commun. **227**, 383 (2003)
31 W.T. Carnall, H. Crosswhite, H.M. Crosswhite, Argone National Laboratory Special Report (1977)
32 W.F. Krupke, IEEE J. Quantum Electron. **QE-10**, 450 (1974)
33 K. Ohta, H. Saito, M. Obara, J. Appl. Phys. **73**, 3149 (1993)
34 D.E. McCumber, Phys. Rev. A **134**, 299 (1964)
35 S.A. Payne, L.L. Chase, L.K. Smith, W.L. Kway, W.F. Krupke, IEEE J. Quantum Electron. **QE-28**, 2619 (1992)
36 F. Güell, J. Gavaldà, R. Solé, J. Appl. Phys. **95**, 919 (2004)
37 S.N. Bagaev, S.M. Vatnik, A.P. Maiorov, A.A. Pavlyuk, D.V. Plakushchev, Quantum Electron. **30**, 310 (2004)
38 W. Ryba-Ramanowski, S. Golab, I. Sololska, G. Dominiak-Dzik, J. Zawadzka, M. Berkowski, J. Fink-Finowicki, M. Baba, Appl. Phys. B **68**, 199 (1999)
39 F. Mougel, K. Dardenne, G. Aka, A. Kahn-Harari, D. Vivien, J. Opt. Soc. Am. B **16**, 164 (1999)